ARTICLE NO. 79-0151R

J80-142

20007
20019

Turbulent Vortices in Stratified Fluids

A. M. Hecht,* A. J. Bilanin,† J. E. Hirsh,‡ and R. S. Snedeker‡
Aeronautical Research Associates of Princeton, Inc., Princeton, N.J.

The effects of density stratification and turbulence on the behavior of vortex rings and vortex pairs is investigated. The results of a vortex ring experiment, in which rings were injected into linear and discontinuous density stratifications, are compared with calculations of ring behavior made using an axisymmetric, unsteady solution of the mean variable and the modeled Reynolds stress equations. Second-order closure of the equations is based upon the invariant modeling technique of Donaldson. Comparisons are made for ring trajectories, radius, and size of the recirculation cell carried along with the ring. Calculations of turbulent vortex pairs descending into a stably stratified atmosphere are presented. The vortex separation for the two-dimensional calculation is found to be very nearly constant with vortex pair descent, while both the experimental and numerical results for vortex rings give a sharply decreasing radius during descent.

Nomenclature

A	= core kinetic energy parameter defined by Eq. (3)
a	= vortex ring oval semimajor axis
b	= vortex ring oval semiminor axis, vortex pair core separation
C_ℓ	= rolling moment coefficient
D	= vortex ring diameter
Fr_1	$= V_0/R_0[g\Delta\rho/\rho_0 R_0]^{1/2}$
Fr_2	$= V_0/NR_0$
Fr_3	$=\Gamma_0/2\pi s^2 N$
g	= gravitational acceleration
N	= Brunt-Vaisala frequency, $[-(g/\rho_0)\mathrm{d}\rho_0/\mathrm{d}z]^{1/2}$ or $[(g/\theta_0)\mathrm{d}\theta_0/\mathrm{d}z]^{1/2}$
q	= root mean square of twice the turbulent kinetic energy
r,z	= radial and axial coordinates of axisymmetric vortex ring calculations, radial coordinate measured from center of vortex pair core
R	= vortex ring radius
s	= vortex pair semiseparation ($2s=b$)
t	= time
V	= vortex ring or pair descent velocity
v	= core swirl velocity
x,y,z	= axial, horizontal, and vertical coordinates of vortex pair
$z_{\max}$	= maximum descent of vortex ring or vortex pair
Γ	= vortex ring or pair circulation
ζ	= vorticity
η	= radial coordinate measured from center of vortex ring core
θ	= mean potential temperature
Λ	= turbulent macroscale
ρ	= density
σ	= spread of core vorticity
ψ	= stream function

Subscripts

avg	= average
0	= initial value
max	= maximum value

Special Symbols

$\langle\ \rangle$	= ensemble averaged

Presented as Paper 79-0151 at the AIAA 17th Aerospace Sciences Meeting, New Orleans, La., Jan. 15-17, 1979; submitted Jan. 22, 1979; revision received Nov. 19, 1979.

Index categories: Jets, Wakes, and Viscid-Inviscid Flow Interactions; Viscous Non-boundary Layer Flows.

*Senior Consultant (now Senior Associate, Continuum Dynamics, Inc.). Member AIAA.

†Senior Consultant (now President, Continuum Dynamics, Inc.). Member AIAA.

‡Associate Consultant. Member AIAA.

I. Introduction

THE hazard created by aircraft trailing vortices has generated renewed interest and research into the physics of vortex flows, concentrating especially upon the behavior of vortex pairs and vortex rings. Experimental studies have been concerned mainly with the latter due to the ease in which they may be generated in the laboratory. The influence of real fluid effects, such as turbulence, on the behavior of vortices has limited the usefulness of purely analytical techniques. We must resort, therefore, to numerical simulations to include these effects.

Vortices in Ideal Fluids

In an ideal constant density fluid without external influences, vortex pairs and vortex rings would persist indefinitely. For a ring with uniform concentrated vorticity, the speed of translation in an ideal fluid has been known for over a century. Kelvin, in 1867, gave the translation velocity for a vortex ring in an ideal fluid as:

$$V=\frac{\Gamma}{4\pi R}\left[\ell n\left(\frac{8R}{\sigma}\right)-\frac{1}{4}\right] \tag{1}$$

where R is the ring radius and σ is the core radius within which the vorticity is uniform. Only recently, the self-induced velocity of translation of vortex rings with arbitrary distribution of vorticity in the core was determined independently by three investigators—Bliss,[1] Saffman,[2] and Fraenkel.[3] The velocity of translation was found to be

$$V=\frac{\Gamma}{4\pi R}\left[\ell n\left(\frac{8R}{\sigma}\right)+A-\frac{1}{2}\right] \tag{2}$$

where A is defined by

$$A=\lim_{\eta/\sigma\to\infty}\int\tilde{v}^2\left(\frac{\eta}{\sigma}\right)\mathrm{d}\left(\frac{\eta}{\sigma}\right)-\ell n\frac{\eta}{\sigma} \tag{3}$$

where $\tilde{v}$ is the swirl velocity nondimensionalized by $\Gamma/4\pi R$, and η is a radius measured from the center of the core (see Fig.

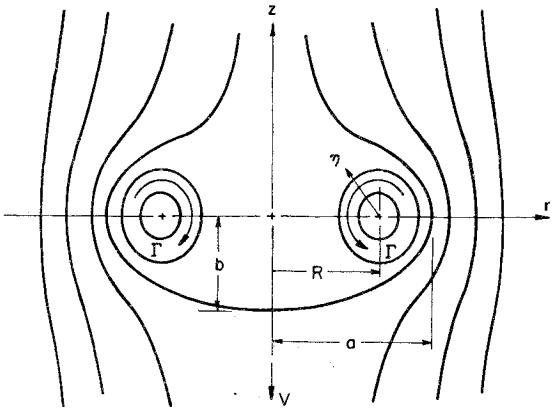

Fig. 1a Vortex ring coordinates and parameters.

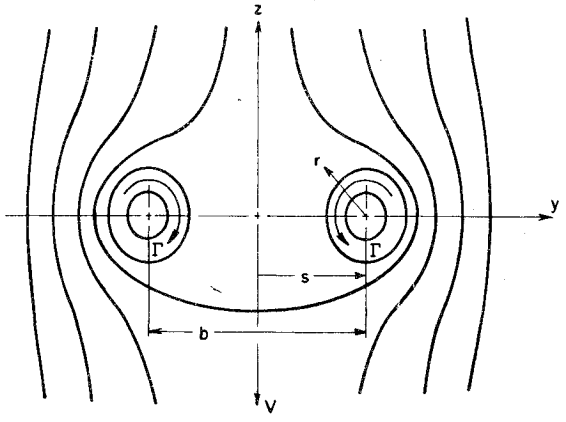

Fig. 1b Vortex pair coordinates and parameters.

1a). For the case of a core with uniform vorticity, $A = 1/4$ for $\sigma/R \ll 1$, recovering Eq. (1).

For a vortex pair with concentrated vorticity, the speed of translation is not critically dependent upon the distribution of vorticity within the core. For a vortex pair with concentrated vorticity in the cores with spread σ, the velocity for core separation b is

$$V = \frac{\Gamma}{2\pi b} + O(\sigma/b)^2 \tag{4}$$

The coordinates for a vortex pair are shown in Fig. 1b.

Vortices in Real Fluids

In the presence of buoyancy, shear, or three-dimensional instabilities, the life time of vortex pairs or vortex rings will be limited by one or more of these effects, and the velocity of translation will no longer obey Eq. (1) or (4) indefinitely. In a real fluid, the action of viscosity and turbulence will limit the distance a vortex attains during descent. The study of aircraft trailing vortices must therefore include the influence of all of these effects, which occur or may occur during the descent of vortices in the real atmosphere.

The role of atmospheric stratification and buoyancy in influencing the behavior of trailing aircraft vortices has been the focus of considerable attention in the recent past.[4-17] The analytical treatments of vortex behavior in stratification provide no clear consensus regarding vortex spacing, descent velocity, and the effect of buoyancy-generated vorticity. Many of the theoretical investigations disregard the effects of viscosity and turbulent transport in their analytic model, although most appear to agree on their importance in controlling the behavior of vortex pairs. The differences in the various models result from how these effects enter into the

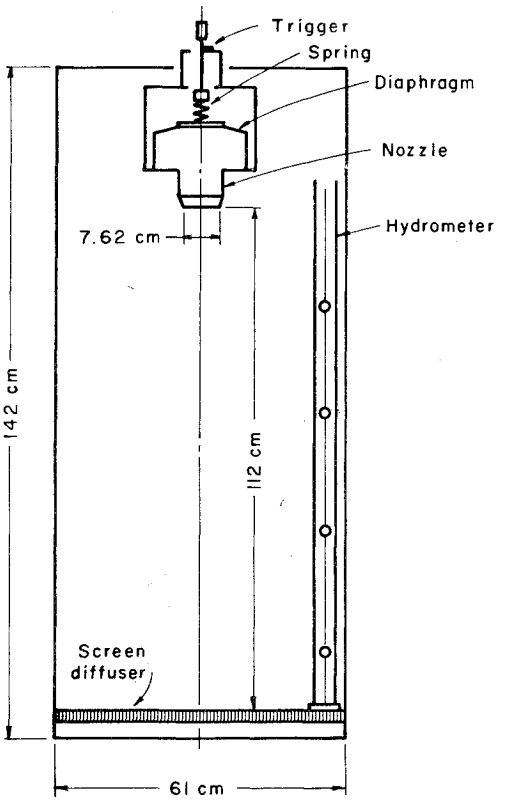

Fig. 2 Vortex ring experimental tank.

physics of the flow and whether any proposed predictive model accounts for the physics correctly.

This is also true in existing analyses of vortex ring behavior. There have been a number of theoretical and experimental investigations of vortex rings, although few have included stratified fluid effects.[14,18-21] As noted by Maxworthy,[19] who conducted vortex ring experiments in a linearly stratified fluid, the complex interactions occurring between the ring dynamics, buoyancy, and turbulent transport cannot be fully accounted for by a simple model. It therefore seems clear that we must resort to numerical calculations which contain a more complete description of these interactions.

The test of any proposed model is, of course, whether it predicts the observed behavior accurately. There are full-scale data available, but little exist which have either been taken under controlled conditions, contain the relevant measurements to validate predictive models sufficiently, or are without ground interference effects. The B-747 aircraft wake vortex tests reported by Burnham et al.[15] provide data taken under controlled conditions and form the basis of a recently completed analysis of stratification effects on vortex wakes.[16]

Laboratory measurements of vortex pair behavior would appear to provide a logical alternative to full-scale experiments to obtain verification of theory. Tomassian[17] has carried out such an experiment in a linearly stratified fluid for a range of Froude numbers. The experimental results indicate that turbulent vortex pairs decelerate in stratification. Vortex pairs generated in a laboratory tank suffer from end wall effects induced by radial inflow in the wall boundary layer, reducing the test time available in which to obtain data free of this influence. The trend of Tomassian's results agree, however, with observed vortex pair behavior in full-scale measurements.

Laboratory study of vortex dynamics is most easily accomplished by observing the behavior of vortex rings. This approach, therefore, offers an alternative in predictive model evaluations and in increasing our understanding of vortex behavior. The following section of this paper contains the

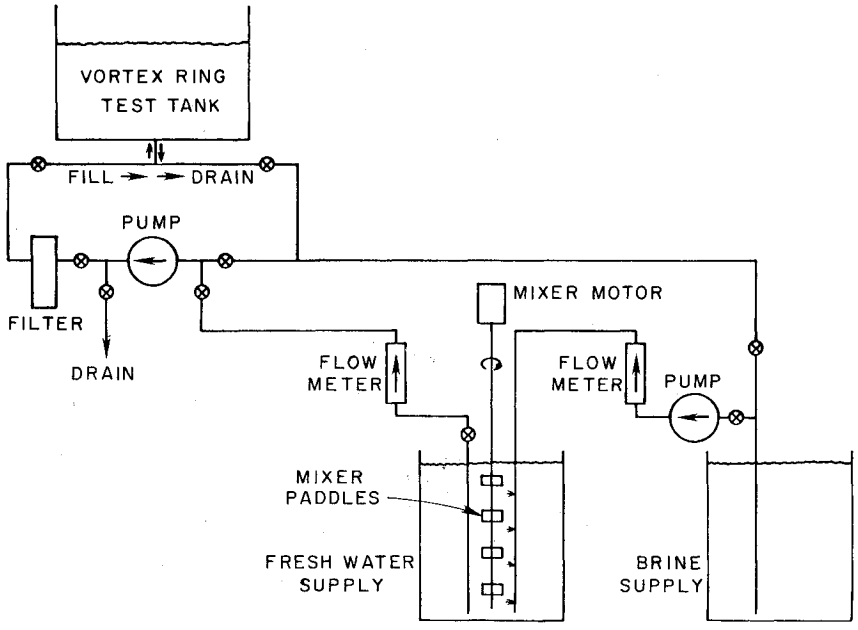

Fig. 3 Schematic of water feed system for producing density stratification.

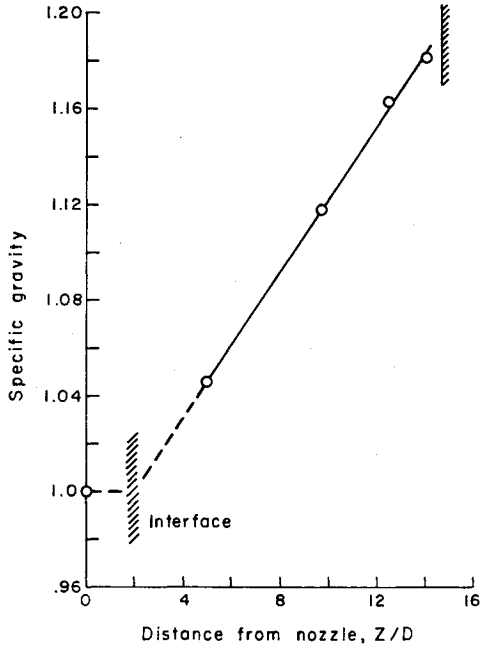

Fig. 4 Measured stratified density of vortex ring experiment.

results of such an experiment and presents a comparison between data and the results of calculations made with an axisymmetric stratified code. This code incorporates the effects of turbulence based upon second-order closure of the Reynolds stress equations, using an invarient model of turbulence transport which has been under development at Aeronautical Research Associates for several years. This work is summarized in an early report by Donaldson,[22] and in more recent reports by Lewellen et al.[23,24] The model has been incorporated into both two-dimensional and axisymmetric computer codes which have been used with considerable success in the study of a variety of stratified wake, aircraft trailing vortex, and meteorological phenomena (see Refs. 13, 16, and 25-28). These codes will be described briefly at appropriate points in the following sections.

II. Vortex Ring Experiment and Calculations

Experimental Apparatus

The apparatus used to perform the vortex ring experiments in a stratified fluid consisted of a transparent test tank, a nozzle-type vortex ring generator, and the necessary mixture tanks, pumps, and piping required to produce a density stratified fluid. A sodium chloride/water brine solution constituted the test medium. A schematic of the tank is shown in Fig. 2, and the system used to produce the stratified brine solution is shown in Fig. 3. A linear density gradient was produced as described by Oster;[29] by setting the brine flow rate at half the flow rate of mixture to the test tank. The initial volume of fresh water was just sufficient to allow the mixture tank to run dry when the test tank was at the desired fill level. A set of hydrometer balls of known specific gravity indicated that, as shown in Fig. 4, the stratification achieved was very nearly linear.

Fluid ejected through the nozzle by a spring loaded diaphragm produced repeatable, well-formed vortex rings. The speed of the rings was controlled by adjusting the spring tension and stroke of the diaphragm. A dye injection system incorporated into the nozzle permitted flow visualization during descent. The tests were recorded using a 16-mm motion picture camera operated at 64 frames/s. Test measurements were then obtained from analysis of the film, with the nozzle orifice providing a reference length for data reduction.

Description of Data

Those experimental cases selected for analysis are listed in Table 1. Also shown are the core spread and maximum vorticity used in initializing the WAKE code calculations. Case 1 was a nonstratified baseline run, cases 2 and 3 were rings of fresh water of specific gravity 1.0 injected into a brine mixture of specific gravity 1.19. The density discontinuity was located approximately three ring diameters below the nozzle exit. Cases 4-6 were conducted in a linearly stratified density fluid. The nozzle was immersed in fresh water and the linear stratification originated at approximately two nozzle diameters below the nozzle exit. This insured rings of known density, since mixing of fluid was anticipated in the nozzle region. The hydrometer ball location before and after each run indicated negligible mixing during the tests. The highly refractive interface existing during the discontinuity test distorted observation in this region although the rings were continuously visible in the linear stratification runs.

Analysis of the flim record provided the ring vertical descent z, diameter D, and the major and minor axes a and b, respectively, of the recirculation cell oval carried along with the ring. Core structure and circumferential velocity could not be measured by this method. The recirculation oval boundary and ring diameter were determined by observation of the dye.

Table 1 Vortex ring experimental and numerical parameters

Case	Stratification	Fr_n [a]	V_0, cm/s	R_0, cm	$z_{max}-z_0$, cm	z_0 cm	$V_0R_0/\nu\times10^{-4}$	σ/R_0	$\zeta_{0_{max}}R_0/V_0$
1	Nonstratified	∞	40.39	4.55	—	12.7	1.81	0.25	22.0
2	Discontinuity	1.27	35.05	4.06	35.5	14.5	1.41		
3	$(\rho/\rho_0=1.19)$	1.36	39.15	4.45	46.7	17.3	1.72	0.25	22.0
4		5.18	23.55	3.23	61.0	12.7	0.75	0.40	10.5
5	Linear	6.17	33.15	3.81	73.5	12.7	1.25	0.30	16.3
6		6.57	38.10	4.11	86.3	12.7	1.55	0.30	16.3

[a] n—Froude number for discontinuous stratification, defined by Eq. (5); for linear stratification, by Eq. (6).

Diffusion time of the dye and decreasing concentration made cell boundary measurements uncertain early and late in each run. In the discontinuity tests, light refraction at the boundary after penetration of the density interface provided definition of the cell, although some uncertainty remained in measurement of the minor axis b due to the wake.

Since three definitions of Froude number were found to be necessary in the present analysis, they are distinguished here by the subscripts 1-3. For the discontinuity tests

$$Fr_1 = V_0\Big/\left[\frac{g\Delta\rho}{\rho_0 R_0}\right]^{1/2} R_0 \tag{5}$$

where $\Delta\rho/\rho_0=0.19$ and R_0 is the initial ring radius before reaching the discontinuity. For the linear density gradient

$$Fr_2 = V_0/NR_0 \tag{6}$$

where

$$N=\left[-\frac{g}{\rho_0}\frac{d\rho_0}{dz}\right]^{1/2}$$

is the Brunt-Väisälä frequency, equal to 1.41 rad/s for the present linear gradient tests. The Froude number used in the analysis of aircraft vortex pairs will be defined in Sec. III.

Shown in Table 1 is the maximum depth of penetration of the rings $(z_{max}-z_0)$, measured to the center of the cell. z_0, measured from the nozzle, is an arbitrarily selected initial point during descent.

The cell size for the nonstratified cases did not change appreciably during descent, and the rings dissipated at the bottom of the test tank. In the stratified cases the oval size decreased appreciably and the rings were destroyed before reaching the bottom of the tank in a catastrophic process as described by Maxworthy.[19]

Description of Axisymmetric Wake Code

The axisymmetric code solves the equations of a second-order closure model of turbulent transport. A second-order model implies that the partial differential equations are solved for the Reynolds stress tensor $\langle u_iu_j\rangle$ as well as for the mean ensemble averaged variables. Higher order unknowns and certain second-order correlations in the Reynolds stress equations have been replaced by modeled terms containing constants and second-order correlations. A derivation of the Reynolds equations for the second-order turbulent correlations and a discussion of the model development and constant evaluation may be found in Lewellen and Teske.[23] The equations were finite differenced on a nonuniformly spaced grid and, with the exception of the equation governing the mean density, solved using a modified ADI scheme. The mean density equation was solved using a flux-corrected transport technique developed by Boris and Book.[30] This was done to improve resolution of the sharp density gradient between the descending oval and the ambient fluid. This gradient increased with time as the ring penetrated progressively further into the stratified environment.

The Poisson equation governing the stream function from which the velocities were obtained was evaluated using a fast elliptic solver developed by Swartztrauber and Sweet.[31] A J6 representation of the convective operator,[32] in which the conservative and nonconservative operators were averaged, was used to improve simulation of the convective nature of the vortex flow problem.

In order to keep the vortex ring in the computational domain, an upwash velocity was added. Following the centroid of the square of the vorticity was used to track the ring.

The computations were initialized by positioning a Gaussian distribution of vorticity of the form

$$\frac{\zeta_0 R_0}{V_0} = \left(\frac{\zeta_{0_{max}}R_0}{V_0}\right)\exp[-(\eta/\sigma)^2] \tag{7}$$

in the aximuthal plane at a point r_0/R_0 and $(z-z_0)/R_0$. These were taken to be 0.95 and 0.0, respectively, since it was found that some roll up of the rings was still occuring at z_0 for most of the measurements.

The radial coordinate η was centered in the vortex core. An isotropic Gaussian spot of turbulence was centered about the vortex core with strength $q_0^2/V_0^2=0.01$ such that

$$\langle uu\rangle=\langle vv\rangle=\langle ww\rangle=(q_0^2/3)\exp[-(\eta/\sigma)^2] \tag{8}$$

The initial conditions are shown schematically in Fig. 5.

At the edges of the computational domain, except at $r=0$, the stream function was evaluated by a moment expansion of the Biot-Savart law.[16] At the inflow boundary at z_- the density was convected in at the appropriate value for the type of stratification considered. The turbulence and vorticity inflow values were set equal to zero. For a linear stratification the density was nondimensionalized by the product of the background gradient and R_0, so that $\partial\rho/\partial z=-1$ non-

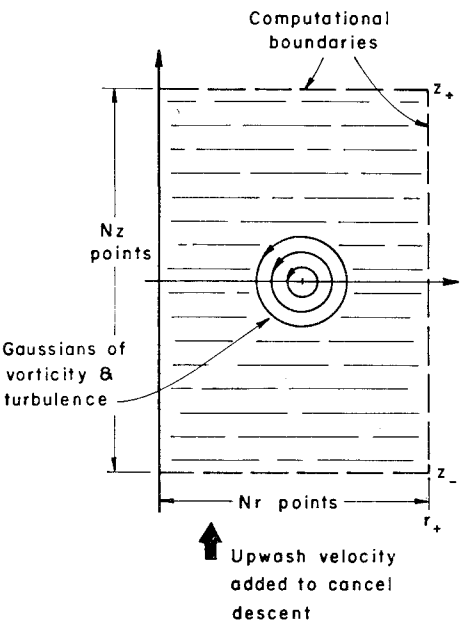

Fig. 5 Schematic representation of axisymmetric WAKE code computational domain and initial conditions.

dimensionally. For the case of the sharp density discontinuity, the total nondimensional density difference across the discontinuity was taken as unity, and the density distribution within the interface was approximated by an error function distribution. At z_+, an advection condition was used to sweep the flow through the outflow boundary. The calculation was terminated when the vertical ring velocity decreased to a value which could not prevent a net inflow velocity over some portion of the z_+ boundary. This prevented calculating the ring descent to zero descent velocity. Because of the relatively high upwash velocity no internal wave interaction problems were encountered at the r_+ boundary. It can be shown by an order of magnitude analysis that the time for waves of typical wavelength to reflect back into the computation was greater by a factor of order $4\pi Fr_2$ than the time for these waves to be swept through the z_+ boundary. For the value of Froude number used in the tests, no reflection problems were encountered.

Because it was not possible to resolve the swirl velocity in and around the core experimentally, another method was devised to obtain the appropriate initial maximum vorticity $\zeta_{0_{\max}}$ and spread σ. This was done by utilizing the measurement of the oval semiaxes a and b (Fig. 1a) and the descent velocity V_0. The semiaxes, which define the separation streamline between fluid carried along with the ring and the ambient fluid, are a function of the core spread σ. Assuming a constant vorticity core, the semiaxes a and b were determined over a range of core radii. Since the descent velocity may be expressed as function of σ and circulation of the ring, it was possible to estimate the circulation from which the maximum vorticity for a Gaussian vorticity distribution could be obtained.

The second-order turbulent closure model contains a dynamic equation for the turbulent macroscale Λ. The calculations presented here were made for a constant scale length and therefore the scale equation was not employed. A parameter study was carried out for a range of values of Λ/R_0 between 0.03 and 0.3. It was found that the former gave closest agreement with the data and this value for the scale was used throughout the vortex ring calculations.

Comparison of Data and Numerical Results

The comparison of experimental data with the numerical results of the stratified axisymmetric code are included in Figs. 6-12. The trajectories of the unstratified and discontinuous density runs (cases 1 and 3) are shown in Fig. 6. Both calculation and experiment show no unusual behavior for the unstratified run. The trajectory for the discontinuity case is almost linear after penetration of the high density interface. This behavior is apparently the consequence of the decrease in ring radius with increasing penetration and the detrainment of

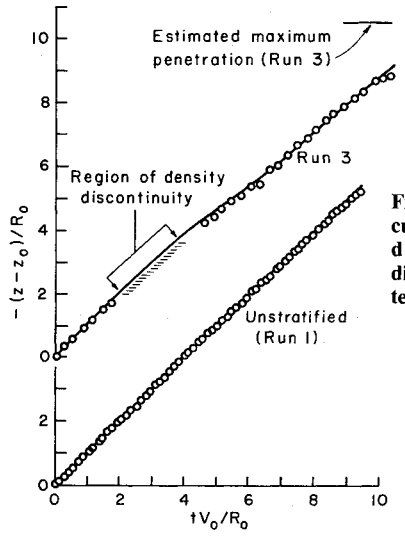

Fig. 6 Comparison of calculated trajectories and data for unstratified discontinuous density vortex ring tests.

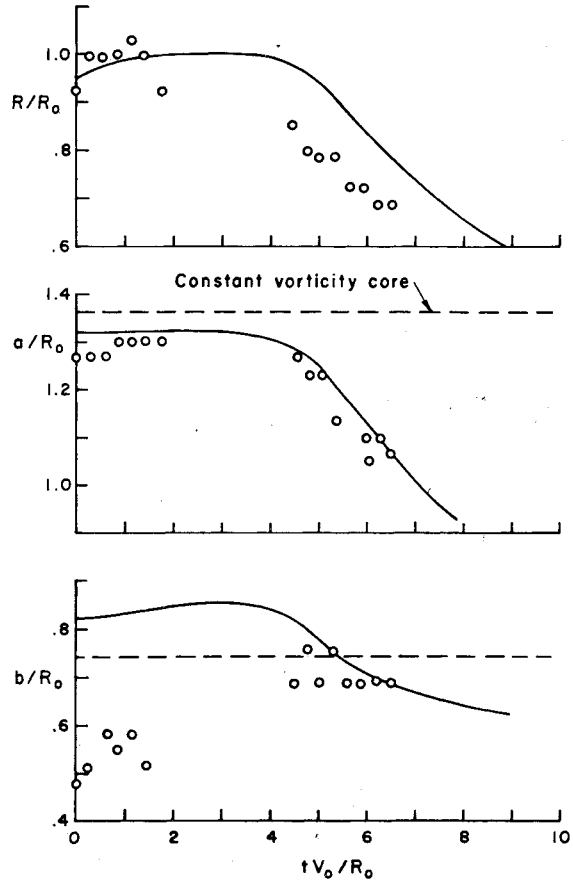

Fig. 7 Comparison of calculated ring radius, semimajor axis a, and semiminor axis b with data for discontinuous density stratification vortex ring test, case 3.

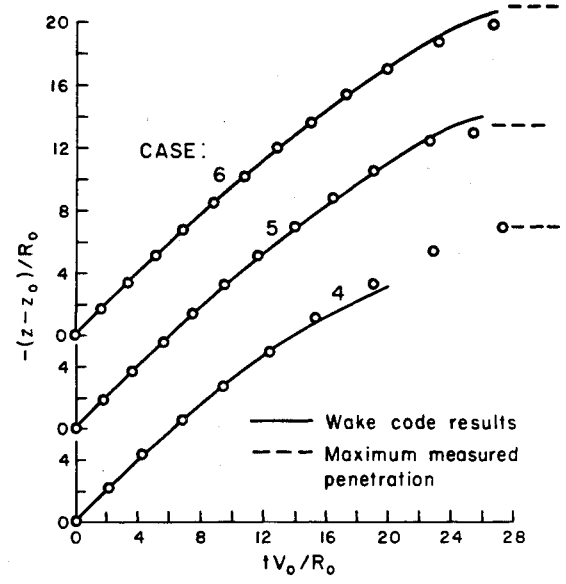

Fig. 8 Comparison of calculated and measured vortex ring trajectories in linear stratification, cases 4-6.

low density fluid from the oval. Figure 7 shows the measured and calculated ring radius and semimajor and semiminor axes. The discrepancy in b/R_0 is possibly due to the failure of the dye to diffuse through the oval at early test times.

The trajectory comparisons for the linear stratification runs are shown in Fig. 8. The numerical simulations for these cases gave excellent agreement over most of the descent, with the possible exception of the lowest injection velocity.

Figure 9 shows the calculated streamlines for case 6, a linear density stratification run. The change in oval size

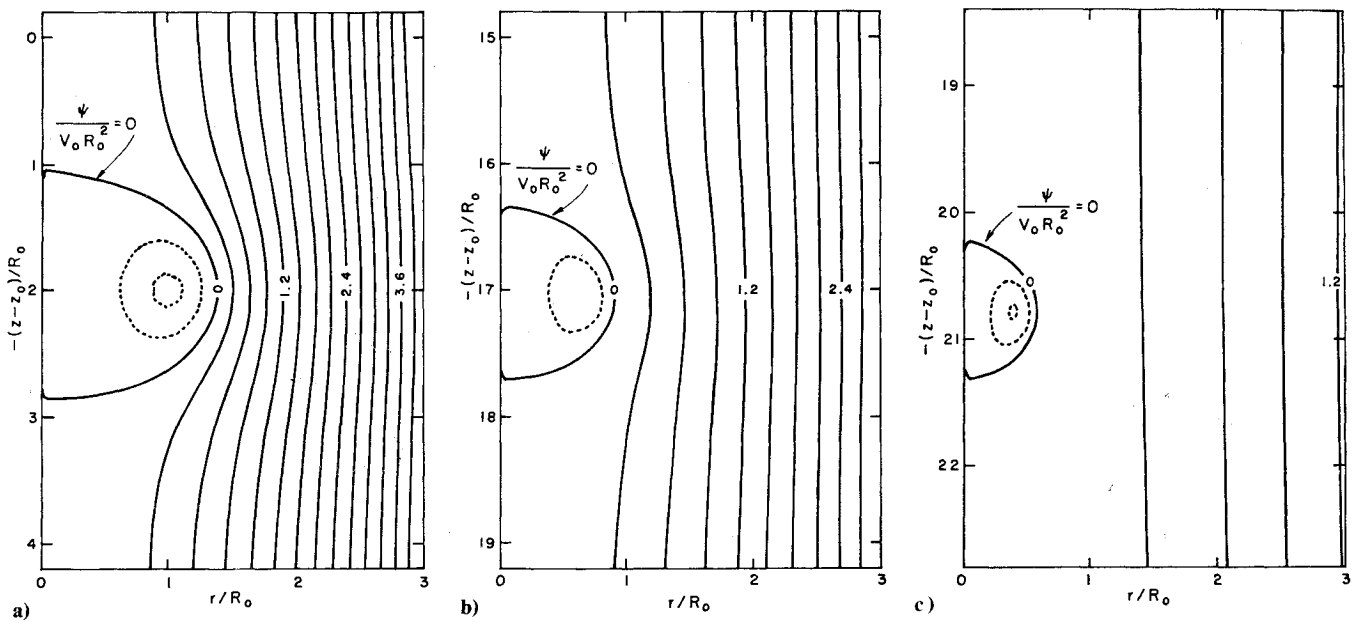

Fig. 9 Calculated vortex ring streamlines for descent into a linearly stratified fluid at $tV_0/R_0 = 2.0$ (a), 20.0 (b), and 27.0 (c).

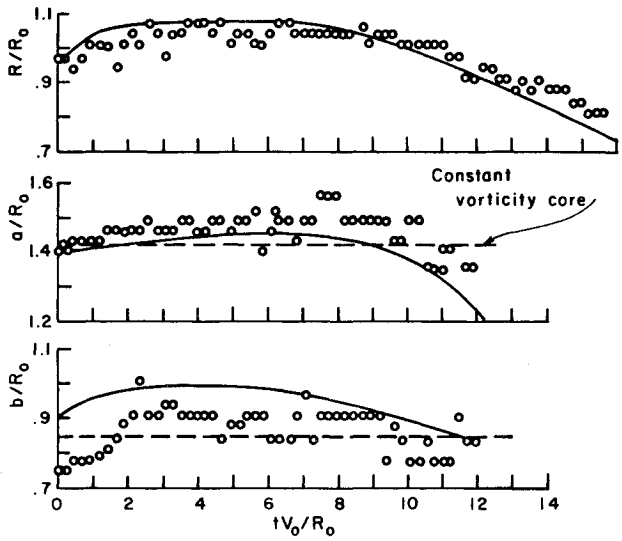

Fig. 10 Comparison of calculated and measured vortex ring radius, semimajor axis a, and semiminor axis b for case 4, linear density stratification.

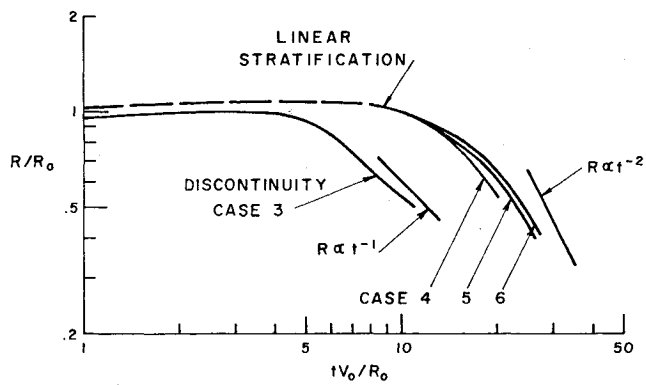

Fig. 11 Calculated vortex ring radius for penetration of density discontinuity and in linear stratification.

during penetration into the stratified fluid was substantial. The calculated horizontal axis of the oval changed by a factor of three by the end of the run. This behavior was also noted experimentally. Figure 10 presents these measurements and the calculated values during the measurable portion of the test for run 4. The lack of data at late test times due to loss of dye makes evaluation of the comparison difficult for the oval axes. The ring radius is predicted well, however. The dependence of calculated radius upon time during penetration into both the discontinuous and linear stratifications is shown in Fig. 11. The ring radius is predicted to behave as t^{-1} for the density discontinuity and as t^{-2} for the linear gradient. The former is confirmed by data (Fig. 12).

III. Vortex Pairs in Stable Atmospheric Stratification

In this section the descent of a vortex pair in a stably stratified atmosphere is investigated. This study is the first which includes turbulent transport directly. Motivation has come from several previously published analytical investigations,[5-12] most of which are in disagreement. This disagreement, as discussed by Widnall,[4] results from different accounting of fluid impulse and energy and the entraining/detraining of mass and vorticity from the interface of the descending oval of fluid. The computations discussed below will suggest that the dynamics of the descent of a vortex pair in a stably stratified flow is intimately tied to correctly accounting for turbulent transport effects.

It is appropriate here to discuss qualitatively the anticipated effects of stratification prior to presenting numerical results. As is well known, a descending vortex pair transports mass downward. This mass is that contained in the oval of recirculating fluid which is observed in a coordinate system moving with the vortex pair. This descent velocity is approximately $\Gamma/4\pi s$. In the absence of three-dimensional instability and ambient atmospheric turbulence, a vortex pair propagates with little change in velocity. If this oval of fluid of density ρ_0 were to descend into a fluid of density ρ_1 such that $\rho_1 > \rho_0$, it is anticipated that the behavior of the pair would be significantly altered as a result of the vorticity generated at the density discontinuity. This generation of vorticity is a consequence of the buoyancy, which appears as a term proportional to $\partial\rho/\partial y$ in the equation governing the evolution of vorticity.

It should be anticipated that the additional vorticity generated will alter the descent of the pair as a consequence of

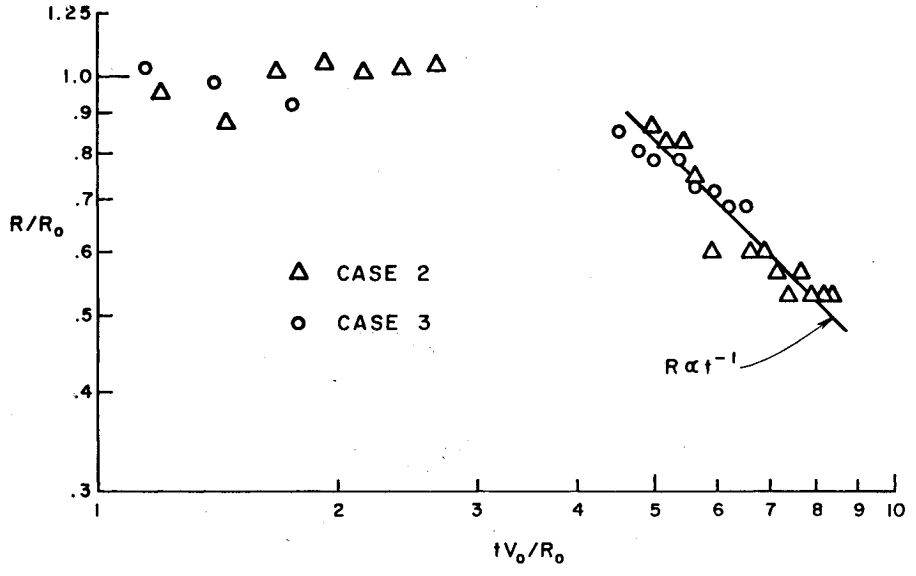

Fig. 12 Measured vortex ring radius for penetration of density discontinuity, cases 2 and 3.

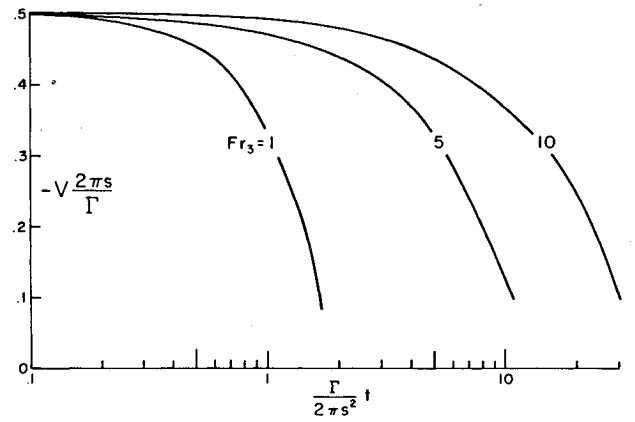

Fig. 13 Calculated velocity of a vortex pair vs time for $Fr_3 = 1$, 5, and 10.

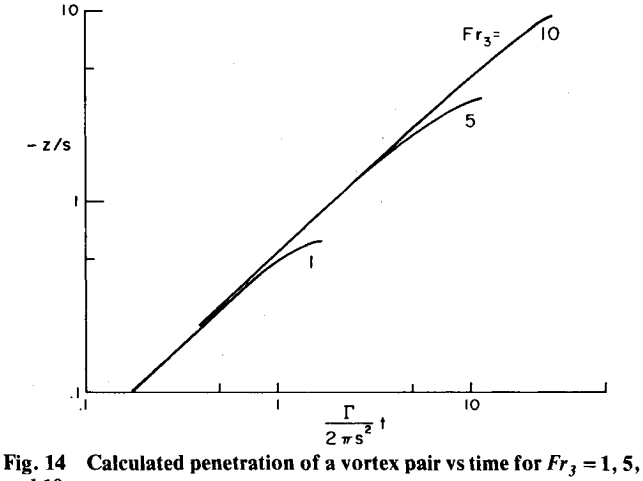

Fig. 14 Calculated penetration of a vortex pair vs time for $Fr_3 = 1$, 5, and 10.

inducing an additional component of velocity on the descending vortices. If the centroids of the buoyancy generated vorticity at the oval boundary are above the pair, the first-order result in the absence of turbulent diffusion is to decrease the vortex pair separation and possibly lead to acceleration.[11] If the centroids were below the pair, the separation would increase, while centroids located at the level of the vortex cores would hold constant separation and decelerate the pair. Unfortunately, turbulent diffusion alters this simple description.

Descent of Vortex Pair in Stably Stratified Atmosphere

The definition of Froude number used in the study of aircraft trailing vortices is

$$Fr_3 = \Gamma/2\pi s^2 N \tag{9}$$

The decay of vortex pairs in a stably stratified atmosphere were simulated at three values of Fr_3, equal to 1.0, 5.0, and 10.0. The calculations were performed using the two-dimensional analog of the axisymmetric code described in the previous section. The solution procedures for the two versions are the same in most respects, except that the vortices are tracked in the two-dimensional version by following the centroid of a passive tracer carried along with the vortices.

The computations were initialized by positioning a Gaussian distribution of vorticity of the form

$$2\pi\zeta s^2/\Gamma = \pm (2s^2/\sigma^2)\exp[-(r/\sigma)^2] \tag{10}$$

at $y/s = \pm 1$, $z/s = 0$, respectively. The coordinate r is measured radially from each vortex center and σ is the vortex spread, which was chosen to be $0.5s$ for the present vortex pair calculations. The numerical mesh is specified only for $y > 0$, since symmetries about $y = 0$ can be utilized.

The initial turbulence distribution was Gaussian with a spread of $0.5s$, and was assumed to be isotropic. The form of the boundary conditions for the two-dimensional solution was the same as that used for the ring calculation. An upwash velocity was again employed to follow the vortex descent. All cases were run with a Reynolds number $Vs/\nu = 10^5$ and a fixed value of the integral scale $\Lambda/s = 0.1$.

Results are shown in Figs. 13 and 14. Figure 13 is a plot of the descent velocity of the vortex measured by tracking the centroid of smoke, while Fig. 14 is a plot of the penetration depth of the vortices as a function of time. Simulations were carried out until the nondimensional descent velocity $2\pi sV/\Gamma$ decreased from an initial value of 0.5 to less than 0.1. Note the much larger total descent, as expected, for the higher Froude number (low stratification) cases. The descent velocity is predicted to be a monotonically decreasing function throughout the computation. Figure 15 shows the evolution of the vortex pair streamlines for $Fr_3 = 10.0$ at $t\Gamma/2\pi s^2 = 0$, 16.0, and 28.0. The oval area is approximately constant until the vortices have nearly stopped descending. This is in sharp contrast with the vortex ring results found both experimentally and numerically in the previous section.

In order to measure the decay rate of the vortices, rolling moments induced on a follower aircraft of wing semispan s_f were computed and are displayed in Fig. 16. It can be seen

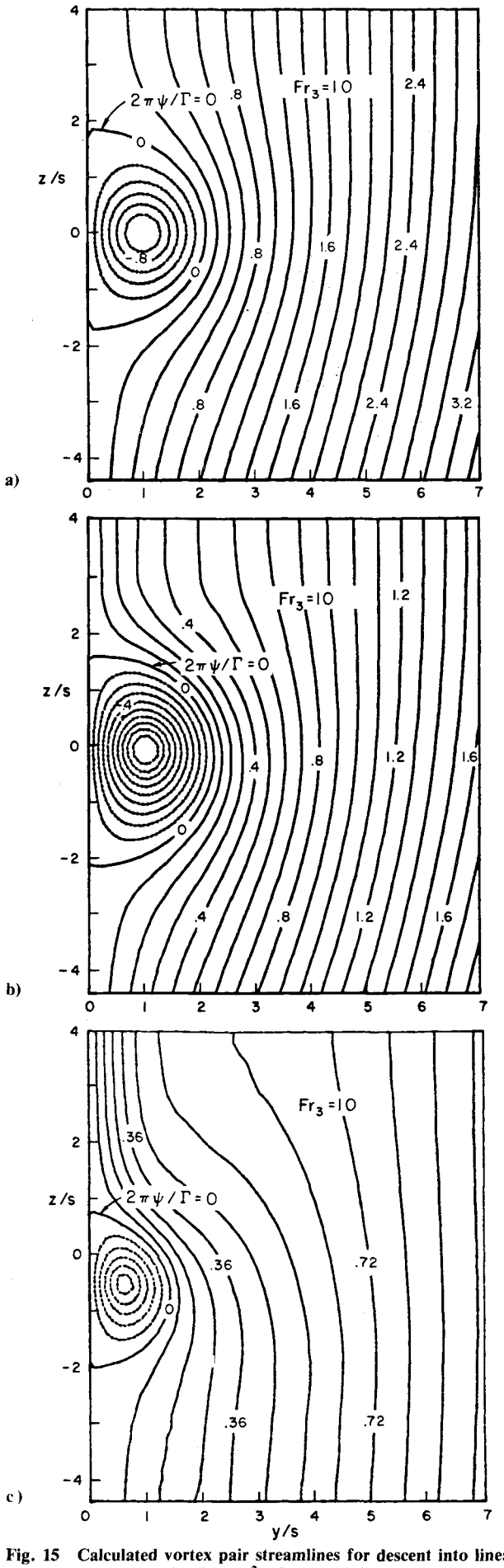

Fig. 15 Calculated vortex pair streamlines for descent into linearly stratified atmosphere for $\Gamma t/2\pi s^2 = 0.0$ (a), 16.0 (b), and 28.0 (c).

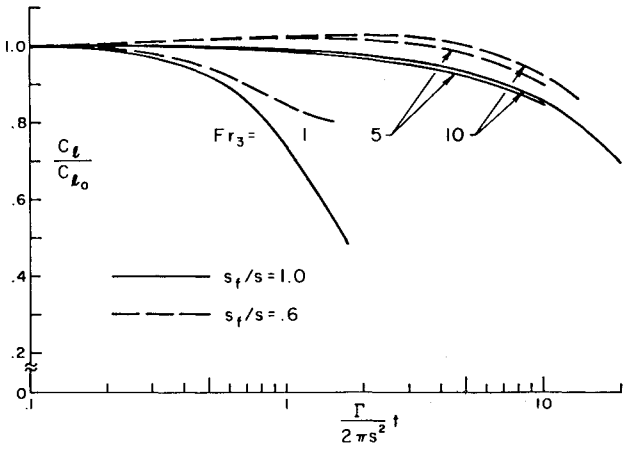

Fig. 16 Calculated rolling moment drop off as function of time for follower aircraft of semispan s_f.

that the vortices have stopped their descent long before there has been any significant decay of rolling moment on the follower aircraft. This is a major finding in that vortices may, as a result of stable stratification, be observed to stop descending but still be capable of inducing large rolling moments on an encountering aircraft.

IV. Conclusions

The following conclusions may be drawn from the present investigation of vortex rings and vortex pairs:

1) Stratification has a profound effect on the radius of a vortex ring descending into a stably stratified fluid. The separation of a vortex pair remains nearly constant until the pair has nearly stopped descending for the parameters used in the calculation shown here.

2) The descent velocity of a vortex ring is nearly constant or decreases monotonically with increasing penetration of a stably stratified fluid, depending upon the type of stratification present (discontinuous or linear). The descent velocity of a vortex pair in linear stratification decreases monotonically. The effects of decreasing radius or separation and the contribution of any countersign vorticity, which may contribute to an acceleration of the pair, cannot overcome the buoyancy in decelerating the recirculation cell. It is apparent that proper accounting for the buoyancy-produced vorticity in predicting the dissipation of a vortex pair in a stably stratified fluid.

A major finding is that once a vortex pair's descent is halted by stratification, the vortex is still capable of inducing a significant rolling moment on an encountering aircraft of a span less than or equal to the generator's span.

Acknowledgments

The bulk of the vortex ring experimental and analytical work reported here was supported by the U.S. Dept. of Transportation System Center under Contract DOT-TSC-1488. The analysis of vortex pairs in stratification was performed for NASA Langley Research Center under Contract NAS1-14707. Construction of the experimental tank was funded by Johns Hopkins University Applied Physics Laboratory as part of Contract APL 600646.

References

[1] Bliss, D. B., "The Dynamics of Curved Rotational Vortex Lines," M.S. Thesis, MIT, Cambridge, Mass., 1970.

[2] Saffman, P. G., "The Velocity of Viscous Vortex Rings," *Studies in Applied Mathematics*, Vol. XLIX, Dec. 1970, pp. 371-380.

[3] Fraenkel, L. E., *Proceedings of Royal Society*, Series A, Vol. 316, 1970, pp. 29-62.

[4] Widnall, S. E., "The Structure and Dynamics of Vortex Filaments," *Annual Review of Fluid Mechanics*, Vol. 7, 1975, pp. 141-165.

[5] Costen, R. C., "Drift of Buoyant Wing-Tip Vortices," *Journal of Aircraft*, Vol. 9, June 1972, pp. 406-412.

[6] Kuhn, G. D. and Nielsen, J. N., "Analytical Studies of Aircraft Trailing Vortices," AIAA Paper 72-42, 1972.

[7] Saffman, P. G., "The Motion of a Vortex Pair in a Stratified Atmosphere," *Studies in Applied Mathematics*, Vol. LI, June 1972, pp. 107-119.

[8] Scorer, R. S. and Davenport, L. J., "Contrails and Aircraft Downwash," *Journal of Fluid Mechanics*, Vol. 43, Pt. 3, 1970, pp. 451-464.

[9] Tombach, I. H., "Transport of a Vortex Wake in a Stably Stratified Atmosphere," *Aircraft Wake Turbulence and its Detection*, edited by J. H. Olsen, A. Goldburg, and M. Rogers, Plenum Press, New York, 1971, pp. 41-57.

[10] Tulin, M. P. and Shwartz, J., "The Motion of Turbulent Vortex Pairs in Homogeneous and Density Stratified Media," Paper presented at 8th ONR Symposium on Naval Hydrodynamics, Calif. Inst. of Technology, Aug. 1970.

[11] Crow, S. C., "Motion of a Vortex Pair in a Stably Stratified Fluid," Poseidon Research Rept. 1, May 1974.

[12] Narain, J. P. and Uberoi, M. S., "The Motion of a Trailing Vortex Wake in a Stratified Medium," *Atmospheric Environment*, Vol. 8, 1974, pp. 459-473.

[13] Bilanin, A. J., Hirsh, J. E., Teske, M. E., and Hecht, A. M., "Atmospheric-Wake Vortex Interaction," NASA Rept. 145336, ARAP Rept. 331, April 1978.

[14] Turner, J. S., "A Comparison between Buoyant Vortex Rings and Vortex Pairs," *Journal of Fluid Mechanics*, Vol. 7, Pt. 3, 1960, pp. 419-432.

[15] Burnham, D. C., Hallock, J. N., Tombach, I. H., Brashears, M. R., and Barber, M. R., "Ground-Based Measurements of a B-747 Aircraft in Various Configurations," U.S. Dept. of Transportation, Rept. FAA-RD-78-146, Dec. 1978.

[16] Hecht, A. M., Bilanin, A. J., Hirsh, J. E., and Snedeker, R. S., "Investigation of Stable Atmospheric Stratification Effect on the Dynamics of Descending Vortex Pairs," U.S. Dept. of Transportation, Rept. FAA-RD-79-10, Feb. 1979.

[17] Tomassian, J. D., "The Motion of a Vortex Pair in a Stratified Medium," Ph.D. Dissertation, Univ. of California at Los Angeles, June 1979.

[18] Linden, P. F., "The Interaction of a Vortex Ring with a Sharp Density Interface: A Model for Turbulent Entrainment," *Journal of Fluid Mechanics*, Vol. 60, Pt. 3, 1973, pp. 467-480.

[19] Maxworthy, T., "Some Experimental Studies of Vortex Rings," *Journal of Fluid Mechanics*, Vol. 81, Pt. 3, 1977, pp. 465-495.

[20] Maxworthy, T., "The Structure and Stability of Vortex Rings," *Journal of Fluid Mechanics*, Vol. 51, Pt. 1, 1972, pp. 15-32.

[21] Maxworthy, T., "Turbulent Vortex Pairs," *Journal of Fluid Mechanics*, Vol. 64, Pt. 2, 1974, pp. 227-239.

[22] Donaldson, C. duP., "Atmospheric Turbulence and the Dispersal of Atmospheric Pollutants," *Proceedings of Workshop on Micrometeorology*, ed. D. A. Haugen, American Meteorology Society, Science Press, 1973, pp. 313-390.

[23] Lewellen, W. S. and Teske, M. E., "Turbulence Modeling and its Application to Atmospheric Diffusion," EPA-600/4-75-016b, 1976.

[24] Lewellen, W. S., Teske, M. E., and Donaldson, C. duP., "Variable Density Flows Computed by a Second-Order Closure Description of Turbulence," *AIAA Journal*, Vol. 14, 1976, pp. 382-387.

[25] Lewellen, W. S., Teske, M. E., and Donaldson, C. duP., "Turbulent Wakes in a Stratified Fluid—Part I: Model Development, Verification and Sensitivity to Initial Conditions," ARAP Rept. 226, Aug. 1974.

[26] Bilanin, A. J., Teske, M. E., and Williamson, G. G., "Vortex Interaction and Decay in Aircraft Wakes," *AIAA Journal*, Vol. 15, Feb. 1977, pp. 250-260.

[27] Bilanin, A. J., Teske, M. E., and Hirsh, J. E., "Neutral Atmospheric Effects on the Dissipation of Aircraft Vortex Wakes," *AIAA Journal*, Vol. 16, Sept. 1978, pp. 956-961.

[28] Lewellen, W. S. and Teske, M. E., "Turbulent Transport Model of Low-Level Winds in a Tornado," Paper presented at 10th American Meterological Society Conference on Severe Local Storms, Oct. 1977.

[29] Oster, G., "Density Gradients," *Scientific American*, Vol. 213, Feb. 1965, pp. 70-76.

[30] Boris, J. P. and Book, D. L., "Flux-Corrected Transport III. Minimal-Error FCT Algorithms," *Journal of Computational Physics*, Vol. 20, 1976, pp. 397-431.

[31] Swartztrauber, P. and Sweet, R., "Efficient Fortran Subprograms of Elliptic Partial Differential Equations," NCAR-TN/LA-109, 1975.

[32] Arakawa, A., "Numerical Simulation of Large Scale Atmospheric Motions in Numerical Solution of Field Problems in Continuum Physics," *SIAM-AMS Proceedings*, Vol. II, 1970, pp. 24-40.